RSC Advances

ROYAL SOCIETY OF CHEMISTRY

www.rsc.org/advances

Journal Name

COMMUNICATION

Strong-Coupled Co-g-C_3N_4/SWCNTs Composites as High-Performance Electrocatalysts for Oxygen Reduction Reaction

Received 00th January 20xx,
Accepted 00th January 20xx

DOI: 10.1039/x0xx00000x

www.rsc.org/

Qiangmin Yu, [a,b,c] Jiaoxing Xu,[a,b] Chuxin Wu,[a,b] and Lunhui Guan* [a,b]

The hybrid materials of cobalt doped graphitic carbon nitride (g-C_3N_4) attached on single-walled carbon nanotubes (SWCNTs) were synthesized by a simple pyrolysis process. Electrochemical measurements revealed that the composities exhibited excellent electrocatalytic activity for oxygen reduction reaction (ORR), with a more positive onset potential (-0.03 V), half-wave potential (-0.15 V), high efficient four-electron process (n=3.97) and much higher stability than that of commercial Pt/C catalysts in alkaline media. The ORR activity mainly originates from the strong coupling of Co-g-C_3N_4 derived active sites on the SWCNTs.

High-performance, low-cost and stabilized electrocatalysts for oxygen reduction reaction (ORR) is urgently needed to renewable energy applications, such as fuel cells and metal-air batteries.[1-3] The ORR, for which is the bottleneck of electrochemical catalytic performance, suffers from a series of problems, including slow charge transfer, low stability under fuel cell and poisoning effects. Currently, the commercial Pt-based materials are considered as the high performance catalyst for ORR, but their high cost, weak tolerance, and scarcity of resources are directly limited its long-term application.[4-6] As a consequence, exploiting non-precious metal catalysts with high ORR activity has become a major challenge in fuel cells. In order to overcome these obstructions, extensive efforts are underway to develop high-activity catalytic materials. Previous studies implied that transition metals (Co, Fe, Mn, etc.) might act as the active sites of the new non-precious metal electrocatalysts.[7-9] However, the sluggish kinetics of non-precious metal catalysts limits the efficiency and performance of the ORR. Recently, carbon-based nanomaterials doped with heteroatoms, especially N-doped carbon materials, have been explored as alternative electrocatalysts for ORR due to their relatively high abundance and low cost.[10-12]

Graphitic carbon nitride (g-C_3N_4) polymer with N-rich and facile synthesis procedure has been proven to provide more active sites than other N-carbon materials for ORR electrocatalysts.[13, 14] However, the catalytic activity of g-C_3N_4 alone is still far inferior to commercial Pt-based catalysts, due to the extremely low electrical conductivity of g-C_3N_4 sheet.[15] With the aim of nitrogen-rich and high conductivity, a variety of carbon materials have been introduced into g-C_3N_4, including carbon black, mesoporous carbon, and graphene oxides.[16-18] But the effect of the structure of these composites is still unknown. Therefore, choosing suitable substrate is a key point to improve the ORR performance of g-C_3N_4.

Single-walled carbon nanotubes (SWCNTs), especially those synthesized by arc-discharged method, due to their high electron conductivity, high specific surface area and integrated structures, are one of the most promising ideal scaffolds for the fabrication of ORR electrocatalyst and Li-insertion materials.[19-21]

Herein we develop a new electrocatalyst, composed of cobalt doped graphitic carbon nitride (Co-g-C_3N_4) and SWCNTs, in which the Co-g-C_3N_4 strong coupled with SWCNTs via π-π interactions. The electrocatalyst displayed excellent electrocatalytic activity and superior stability, resultant from the strong-coupling of Co-g-C_3N_4 and SWCNTs, thus making it as the promising candidate for the non-precious metal ORR catalysts.

Microscopic structure analyses of the Co-g-C_3N_4/SWCNTs samples with respect to pure-SWCNTs were performed by transmission electron microscopy (TEM), as displayed in Figure1a-b. Compared to the bare surface of pure-SWCNTs (**Fig. 1a**), the Co-g-C_3N_4/SWCNTs demonstrate homogeneous distribution of Co-g-C_3N_4 on SWCNTs, as observed clearly in **Fig. 1b**. The uniform dispersion of C, N and Co elements was also observed in elemental-mapping (see **Fig. S1** for detail information). It should be noted that without cobalt anticipation, the size of g-C_3N_4 particles on the SWCNTs appear severe aggregation (**Fig. 1c**). It implied that the metal cobalt helpfully disperse the pyrolyzed g-C_3N_4 on the SWCNTs. The HR-TEM image of Co-g-C_3N_4 nanosheet (inset in **Fig. 1b**) reveals clear

[a] Qiangmin Yu, Jiaoxing Xu, Chuxin Wu, and Prof. Lunhui Guan
Key Laboratory of Design and Assembly of Functional Nanostructures, Fujian Institute of Research on the Structure of Matter, Chinese Academy of Sciences, YangQiao West Road 155#, Fuzhou, Fujian 350002, P.R. China.
Fax: (+) 86-591-6317 3550; Tel: 86-591-6317 3550;
E-mail: guanlh@fjirsm.ac.cn
[b] Qiangmin Yu, Jiaoxing Xu, Chuxin Wu, and Prof. Lunhui Guan
Fujian Key Laboratory of Nanomertials, Fuzhou, Fujian 350002, China
[c] Qiangmin Yu
University of Chinese academy of sciences, Beijing 100049, China
† Footnotes relating to the title and/or authors should appear here.
Electronic Supplementary Information (ESI) available: [details of any supplementary information available should be included here]. See DOI: 10.1039/x0xx00000x

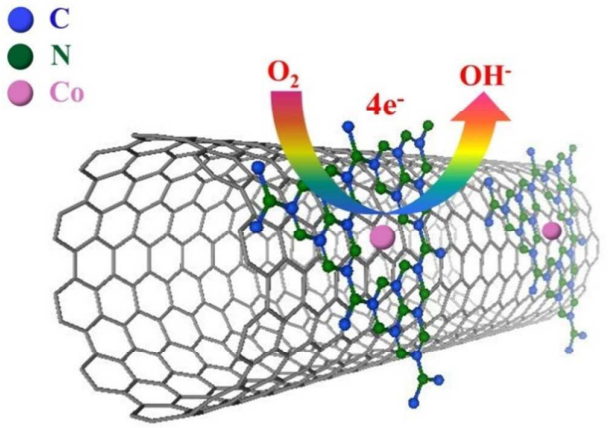

Scheme. 1 Schematic presentations showed the ORR on the envisaged microstructures of Co-g-C_3N_4/SWCNTs.

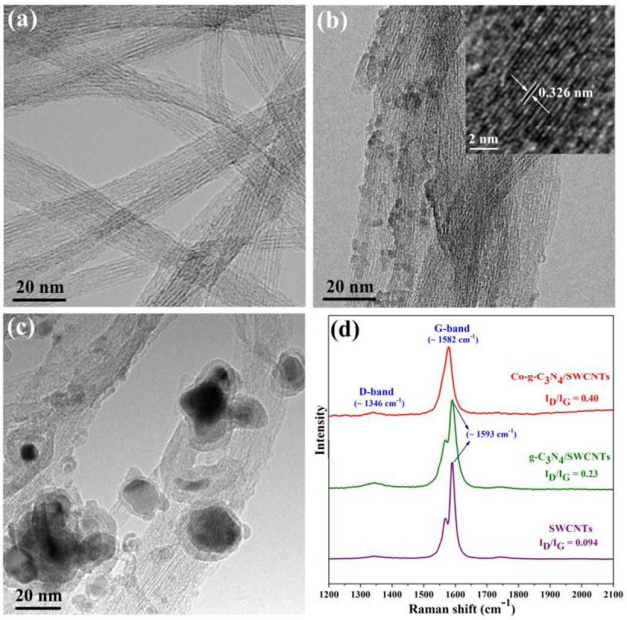

Fig. 1 (a) TEM images of the pure-SWCNTs, (b) TEM image of the Co-g-C_3N_4/SWCNTs composites (inset: the HRTEM image of Co-g-C_3N_4 nanosheet), (c) TEM image of the g-C_3N_4/SWCNTs composites, (d) Raman spectrum of the pure-SWCNTs, g-C_3N_4/SWCNTs and the Co-g-C_3N_4/SWCNTs composites.

lattice fringes with a distance of 0.326 nm, corresponding to the (002) plane of g-C_3N_4.[22] The reduced crystal size of Co-g-C_3N_4/SWCNTs was also confirmed by XRD, as comparatively displayed in **Fig. S2**. Compared to the pure-g-C_3N_4 at 27.4°, the (002) diffraction peak of Co-g-C_3N_4 shows a significant decrease in intensity, indicating the reduce layers of g-C_3N_4 nanosheet. Together with the absence of (100) peak at 13.2°, it confirmed that cobalt ions are embedded into graphitic carbon nitride networks.[23] For the Co-g-C_3N_4/SWCNTs, the (002) diffraction peak at 27.4° of g-C_3N_4 disappeared, while a new diffraction peak assigned to a layer to tube distance between Co-g-C_3N_4 and SWCNTs appears at 26.6°. All these indicate that the Co-doped g-C_3N_4 is well dispersing on SWCNTs with a strong interaction. Nitrogen physisportion of Co-g-C_3N_4/SWCNTs was measured to investigate the surface structure (**Fig. S3-a**). The Brunauer-Emmett-Tellersurface areas are 426 $m^2 g^{-1}$ and the diameters of the pores are in the range of 1.2 to 30 nm. The surface areas of Co-g-C_3N_4/SWCNTs are higher than that of pure-SWCNTs (166 $m^2 g^{-1}$, **Fig. S3-b**), which might derive from the melamine pyrolysis. Moreover, the presence of micro-pores (< 2 nm) is beneficial to the formation of metal-nitrogen active sites in catalysts.[24, 25]

Raman spectroscopy was used to detect the charge transfer between the Co-g-C_3N_4 and SWCNTs. The Raman results of pure SWCNTs, g-C_3N_4/SWCNTs and Co-g-C_3N_4/SWCNTs are shown in **Fig. 1d**. The Raman peaks centered at about ~ 1346 cm^{-1} and ~ 1593 cm^{-1} are attributed to the D and G bands of SWCNTs, respectively.[26] It is well-known that the frequency of G band is sensitive to the interfacial charge transfer.[27] After being incorporated with Co-g-C_3N_4, the G band of SWCNTs red shifted (approximately 11 cm^{-1}) obviously, due to the charge transfer between the Co-g-C_3N_4 and the host SWCNTs. For Co-g-C_3N_4/SWCNTs composites, Co-g-C_3N_4 can bind to the SWCNTs sidewall via strong π-π stacking interaction, which promote electron-transfer between Co-g-C_3N_4 and the host SWCNTs.[28] On the contrary, when SWCNTs were coupled with undoped g-C_3N_4, the G band shifted barely. It confirmed that Co embedded into graphitic carbon nitride greatly enhanced the charge transfer between Co-g-C_3N_4 and SWCNTs. The intensity of D band normalized toward G band (I_D/I_G) was used to measure the disorder degree of SWCNTs in three samples. The Co-g-C_3N_4/SWCNTs sample has an I_D/I_G ratio of 0.40, which is much higher than that of the original pure SWCNTs (0.094) and that of the g-C_3N_4/SWCNTs (0.23). The results indicated the higher defects concentration of the SWCNTs in Co-g-C_3N_4/SWCNTs.

As expected, X-ray photoelectron spectroscopy (XPS) shows the existence of carbon, oxygen, nitrogen and cobalt (**Fig. 2a**). The O 1s peak most likely arises from the incorporation of physicochemical absorbed oxygen and trace amounts of metal-oxygen coordination. The high resolution N 1s spectrum reveals with several N species at different binding energy (**Fig. 2b**). The dominant peak at 398.6 eV corresponds to the sp^2-bonded N atoms in triazine rings (C-N=C).[29] The peak at 400.8 eV can be assigned to N atoms in triazine rings and N $(-C)_3$.[30, 31] The Co 2p XPS spectrum of Co-g-C_3N_4/SWCNTs can be deconvoluted into two peaks with binding energies of 781.3 and 795.8 eV (**Fig. 2c**), which correspond to nitrogen- and oxygen-coordinated metals, respectively.[30, 32-34] The Co-g-C_3N_4/SWCNTs samples with a high N content (~15.2 at %) might benefit from the coordinative Co-g-C_3N_4 structure. A referenced sample of g-C_3N_4/SWCNTs was also measured to prove Co-N coordination. The N content of g-C_3N_4/SWCNTs (~8.7 at %) are much lower than that of Co-g-C_3N_4/SWCNTs. Moreover, the Co/N atomic ratio of Co-g-C_3N_4/SWCNTs was calculated to be 0.13, higher than that of bulk Co-g-C_3N_4 (0.09), suggesting a more stable Co-g-C_3N_4 substructure originated from the potential electronic coupling

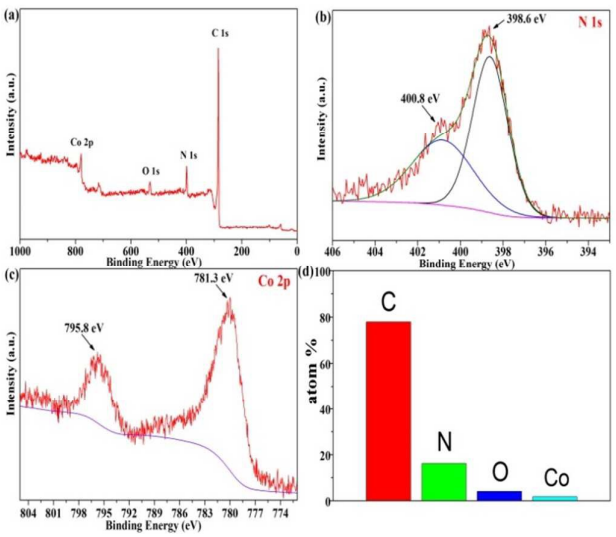

Fig. 2 (a) The XPS survey spectra (0-1000 eV) of Co-g-C_3N_4/SWCNTs, (b) N 1s spectrum, (c) Co 2p spectrum, and (d) each atom contents of Co-g-C_3N_4/SWCNTs.

between SWCNTs and Co-g-C_3N_4. The high Co/N atomic ratio can be attributed to the nitrogen transfer from g-C_3N_4 to SWCNTs during the pyrolysis of melamine.[15, 31, 35] To further demonstrate that the cobalt embedded into g-C_3N_4, the Co- g-C_3N_4/SWCNTs composites were washed by1 mol/L HCl (50 ml) solution at 50 °C for 6 h. The Co spectrum was shown in **Fig. S4.** With respect to the Co-g-C_3N_4/SWCNTs, the pickling composites peak intensity (at 795.8 eV) decreases significantly, while the peak intensity (at 781.3 eV) decreases barely.

The cathodic ORR electrocatalytic properties of Co-g-C_3N_4/SWCNTs were estimated in a three-electrode system at room temperature. Firstly, the cyclic voltammetry of Co-g-C_3N_4/SWCNTs was performed in both O_2 and N_2-saturated 0.1 M NaOH solution (**Fig. 3a**). CV curves show no any significant peak in the N_2-saturated electrolyte. On the contrary, a characteristic ORR peak at about -0.22 V was observed in the presence of oxygen, indicating the electrocatalytic activity of Co-g-C_3N_4/SWCNTs for ORR. The current response shows a weak oxidation peak at 1.9 V, possibly due to the cobalt ions transform from low valent state to high valent state. For understanding the strong coupling of Co-g-C_3N_4 component and SWCNTs in Co-g-C_3N_4/SWCNTs catalysts, the ORR performance of referred samples of g-C_3N_4, Co-g-C_3N_4, SWCNTs and g-C_3N_4/SWCNTs were also measured. As displayed in **Fig. 3b** and **Fig. S5**. The largest ORR peak-current and most positive ORR peak-potential on the Co-g-C_3N_4/SWCNTs electrode suggest the highest ORR activity for Co-g-C_3N_4/SWCNTs as compared to the g-C_3N_4, Co-g-C_3N_4, SWCNTs and g-C_3N_4/SWCNTs catalysts. The results indicated that the electrocatalytic activity originates from the Co-g-C_3N_4 derived active sites and SWCNTs with a high conductivity. The composites cyclic voltammograms shows a half-wave potential of -0.163V, much more positive than the reported g-C_3N_4@carbon catalyst in 3D structure, [16, 18] and comparable to those of the state-of-the-art commercial noble-metal catalysts.[36]

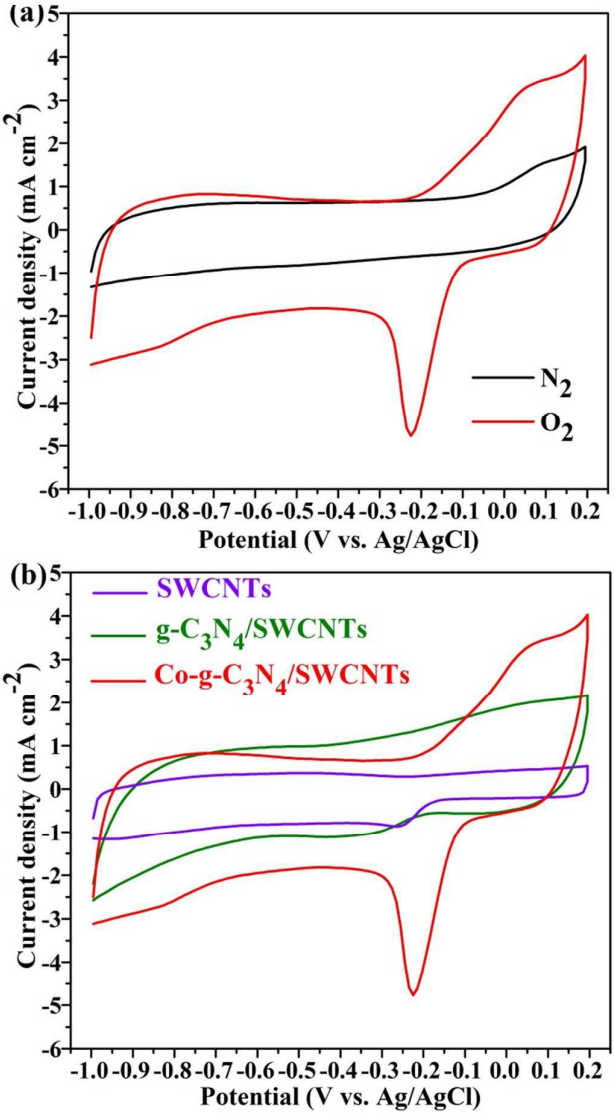

Fig. 3 (a) Cyclic voltammograms of the Co-g-C_3N_4/SWCNTs composites at a scan rate of 50 mV s^{-1} in 0.1 M NaOH solution saturated with N_2 (black curves) and O_2 (red curves). (b) Cyclic voltammograms of SWCNTs, g-C_3N_4/SWCNTs, and Co-g-C_3N_4/SWCNTs with a scan rate of 50 mV s^{-1}.

To further confirm the strong coupling of Co-g-C_3N_4 and SWCNTs, linear sweep voltammetry (LSV) were performed on bulk Co-g-C_3N_4, g-C_3N_4/SWCNTs Co-g-C_3N_4/SWCNTs samples in comparison to commercial Pt/C (**Fig. 4**). The electrochemical catalytic performance parameters are summarized in the Table S1. Among the three C_3N_4-based ORR catalysts, the Co-g-C_3N_4/SWCNTs presents most positive onset potential (-0.03 V) and half-wave potential (-0.15 V), comparable to the commercial Pt/C catalyst. More importantly, the Co-g-C_3N_4/SWCNTs displays apparently better ORR current density with respect to bulk Co-g-C_3N_4 and the Co free g-C_3N_4/SWCNTs. This indicates the strong coupling of Co-g-C_3N_4 and SWCNTs.

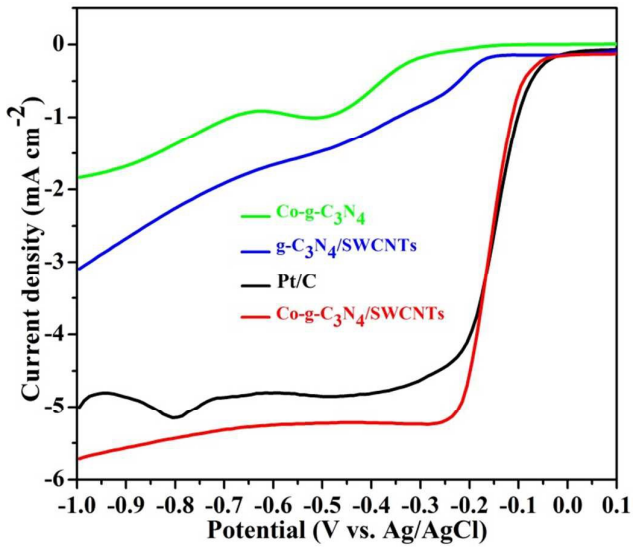

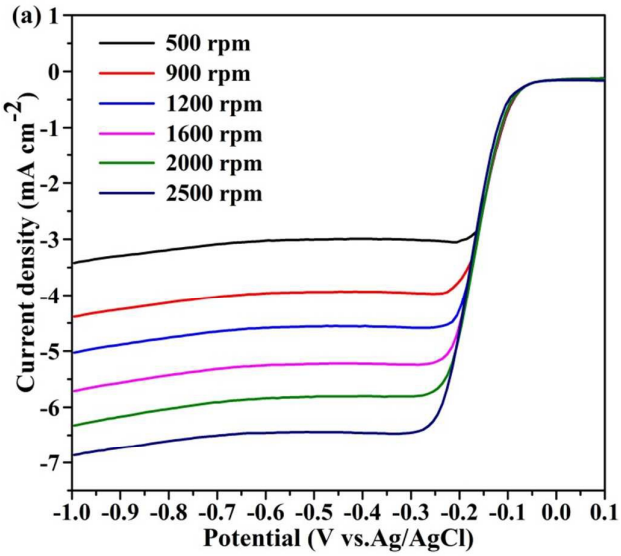

Fig. 4 Linear sweep voltammetry curves of different samples with Pt/C in comparison in an O_2-saturated 0.1 M NaOH solution at a scan rate of 10 mV s^{-1} and 1600 rpm.

To gain further insight into the role of Co-g-C_3N_4/SWCNTs during the ORR electrochemical process, the reaction kinetics was studied by rotation disk voltammetry. **Fig. 5a** shows RDE current-potential curves at different rotation rates for Co-g-C_3N_4/SWCNTs electrodes in the O_2-saturated 0.1 M NaOH electrolyte. The measured current density shows the typical increase with increasing rotation rate (from 500 to 2500 rpm). The transferred electron number of per O_2 molecule for ORR was determined by the Koutecky-Levich equation given below: [37, 38]

$$\frac{1}{j} = \frac{1}{j_k} + \frac{1}{B\omega^{1/2}}$$

Where j_k is the kinetic current and ω is the electrode rotation rate. B would be determined from the slope of K-L plots (**Fig. 5b**) based on Levich equation as follows:

$$B = 0.62nFA\left(D_{O_2}\right)^{2/3}v^{-1/6}C_{O_2}$$

In which n represents the number of electrons transferred per O_2 molecule; F is the Faraday constant (F= 96485 C mol^{-1}); A is the geometric electrode area (0.196 cm^2); D_{O_2} is the diffusion coefficient of O_2 in 0.1 M NaOH solution (1.9 × 10^{-5} cm^2 s^{-1}); v is the kinetic viscosity (0.01 cm^2 s^{-1}); and C_{O_2} is the bulk concentration of the O_2 in 0.1 M NaOH solution (1.2 × 10^{-6} mol cm^{-3}). The constant 0.62 is adopted when the rotation rate expressed in rad s^{-1}.

The Koutecky-Levich equation corresponding curves are plotted for different potentials in **Fig. S8**. The n value for Co-g-C_3N_4/SWCNTs was calculated to be 3.97 at the potential of -0.35 V, comparable to that of Pt/C (n=3.91, calculated from **Fig. S6**), suggesting a high efficient four-electron process for the ORR on the Co-g-C_3N_4/SWCNTs electrode. From the slope of the Koutecky-

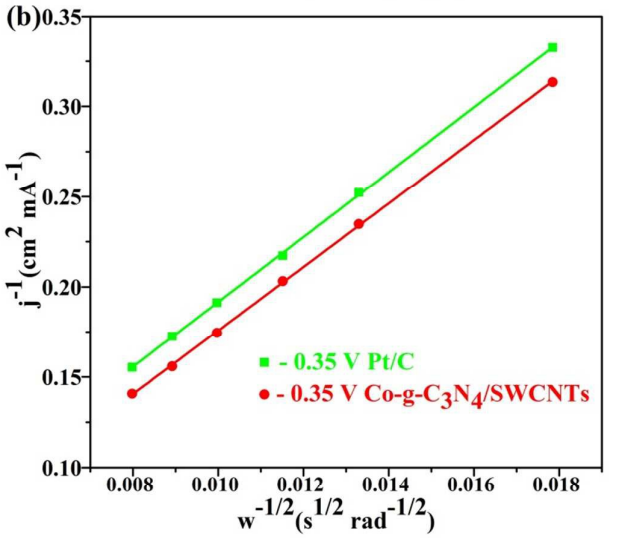

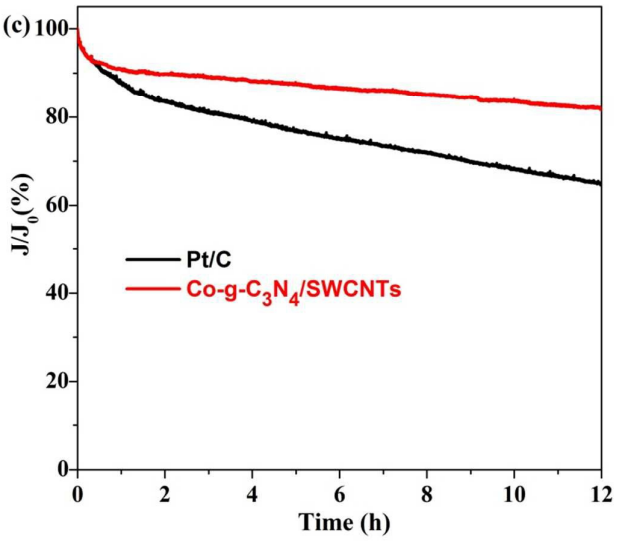

Fig. 5 (a) Linear sweep voltammetry curves of Co-g-C_3N_4/SWCNTs in an O_2-saturated 0.1 M NaOH solution at a sweep rate of 10 mV s^{-1} under various rotation rates. (b) Koutecky-Levich plot for Co-g-C_3N_4/SWCNTs and Pt/C at -0.35 V obtained from Fig. 5a and Fig. S6, respectively. (c) Current-Time chronoamperometric response of Co-g-C_3N_4/SWCNTs and Pt/C in O_2-saturated 0.1 M NaOH solution at a rotation rate of 1600 rpm.

Levich plots (**Fig. S8**) derived from the data in **Fig. 5a**. The parallel and straight fitting lines of 1/j vs $1/\omega^{0.5}$ imply a first-order reaction toward dissolved oxygen. The n value for Co-g-C_3N_4/SWCNTs is derived to be 3.90-3.97 at the potential ranging from-0.25 to -0.45 V (**Fig. S8**). This further confirmed the high ORR efficiency of Co-g-C_3N_4/SWCNTs. In addition, the n value of Co-g-C_3N_4/SWCNTs also confirmed by RRDE results (**Figure S9**, Supporting Information). The Co-g-C_3N_4/SWCNTs also exhibited an ORR process approximating a 4e transfer pathway.

In order to test the stability of the electrocatalytic activity, a chronoamperometry at -3.0 V in O_2-saturated 0.1 M NaOH electrolyte at a rotation rate of 1600 rpm was carried out for 12 h. As shown in **Fig. 5c**, the corresponding current-time chronomperometric response of Co-g-C_3N_4/SWCNTs exhibits a very slow attenuation and a high relative current of 82.3% still persists after 12 h. The stability of Co-g-C_3N_4/SWCNTs higher than that of the graphene supported Co-g-C_3N_4,[29] confirming a strong coupling between Co-g-C_3N_4 and SWCNTs on the Co-g-C_3N_4/SWCNTs catalyst. In contrast, commercial Pt/C shows a gradual decrease with a current loss of approximately 35.5% measured after 12 h. This result clearly suggests that the durability of Co-g-C_3N_4/SWCNTs catalysts is superior to that of the Pt/C catalyst.

Conclusions

In summary, we have successfully synthesized a high-performance electrocatalyst coupled by Co-g-C_3N_4 and SWCNTs. The ORR activity for Co-g-C_3N_4/SWCNTs electrocatalyst arises from the Co-g-C_3N_4 derived active sites and the excellent conductivity of SWCNTs. Within the context of simple synthesis, more positive onset potential, number of electron transfer and the reliable stability, the Co-g-C_3N_4/SWCNTs Composites actually exhibited remarkable ORR performance compared to commercial Pt/C catalysts. All these superior properties make Co-g-C_3N_4/SWCNTs a potentially promising and suitable substitute for Pt/C catalyst, especially in alkaline fuel cell.

Notes and references

1. R. F. Service, *Science*, 2009, 324, 1257-1259.
2. T. Ogasawara, A. Debart, M. Holzapfel, P. Novak and P. G. Bruce, *Journal of the American Chemical Society*, 2006, 128, 1390-1393.
3. N. S. Lewis, *Science*, 2007, 315, 798-801.
4. R. Bashyam and P. Zelenay, *Nature*, 2006, 443, 63-66.
5. H. A. Gasteiger and N. M. Markovic, *Science*, 2009, 324, 48-49.
6. M. K. Debe, *Nature*, 2012, 486, 43-51.
7. Y. Y. Liang, H. L. Wang, P. Diao, W. Chang, G. S. Hong, Y. G. Li, M. Gong, L. M. Xie, J. G. Zhou, J. Wang, T. Z. Regier, F. Wei and H. J. Dai, *Journal of the American Chemical Society*, 2012, 134, 15849-15857.
8. G. Wu, K. L. More, C. M. Johnston and P. Zelenay, *Science*, 2011, 332, 443-447.
9. Y. Y. Liang, Y. G. Li, H. L. Wang, J. G. Zhou, J. Wang, T. Regier and H. J. Dai, *Nature Materials*, 2011, 10, 780-786.
10. D. S. Su, S. Perathoner and G. Centi, *Chemical Reviews*, 2013, 113, 5782-5816.
11. M. M. Liu, R. Z. Zhang and W. Chen, *Chemical Reviews*, 2014, 114, 5117-5160.
12. K. P. Gong, F. Du, Z. H. Xia, M. Durstock and L. M. Dai, *Science*, 2009, 323, 760-764.
13. S. M. Lyth, Y. Nabae, S. Moriya, S. Kuroki, M. Kakimoto, J. Ozaki and S. Miyata, *Journal of Physical Chemistry C*, 2009, 113, 20148-20151.
14. X. Wang, L. Wang, F. Zhao, C. Hu, Y. Zhao, Z. Zhang, S. Chen, G. Shi and L. Qu, *Nanoscale*, 2015, 7, 3035-3042.
15. S. B. Yang, X. L. Feng, X. C. Wang and K. Mullen, *Angew Chem Int Edit*, 2011, 50, 5339-5343.
16. J. Liang, Y. Zheng, J. Chen, J. Liu, D. Hulicova-Jurcakova, M. Jaroniec and S. Z. Qiao, *Angewandte Chemie-International Edition*, 2012, 51, 3892-3896.
17. K. Kwon, Y. J. Sa, J. Y. Cheon and S. H. Joo, *Langmuir*, 2012, 28, 991-996.
18. Y. Zheng, Y. Jiao, J. Chen, J. Liu, J. Liang, A. Du, W. M. Zhang, Z. H. Zhu, S. C. Smith, M. Jaroniec, G. Q. Lu and S. Z. Qiao, *Journal of the American Chemical Society*, 2011, 133, 20116-20119.
19. Y. A. Kim, M. Kojima, H. Muramatsu, S. Umemoto, T. Watanabe, K. Yoshida, K. Sato, T. Ikeda, T. Hayashi, M. Endo, M. Terrones and M. S. Dresselhaus, *Small*, 2006, 2, 667-676.
20. A. N. Golikand, M. Asgari, E. Lohrasbi and M. Yari, *J Appl Electrochem*, 2009, 39, 1369-1377.
21. J. X. Li, Y. Zhao and L. H. Guan, *Electrochem Commun*, 2010, 12, 592-595.
22. F. Dong, L. W. Wu, Y. J. Sun, M. Fu, Z. B. Wu and S. C. Lee, *Journal of Materials Chemistry*, 2011, 21, 15171-15174.
23. M.-Q. Wang, W.-H. Yang, H.-H. Wang, C. Chen, Z.-Y. Zhou and S.-G. Sun, *ACS Catalysis*, 2014, 4, 3928-3936.
24. H. W. Liang, W. Wei, Z. S. Wu, X. L. Feng and K. Mullen, *J Am Chem Soc*, 2013, 135, 16002-16005.
25. N. Ramaswamy, U. Tylus, Q. Y. Jia and S. Mukerjee, *J Am Chem Soc*, 2013, 135, 15443-15449.
26. A. M. Rao, E. Richter, S. Bandow, B. Chase, P. C. Eklund, K. A. Williams, S. Fang, K. R. Subbaswamy, M. Menon, A. Thess, R. E. Smalley, G. Dresselhaus and M. S. Dresselhaus, *Science*, 1997, 275, 187-191.
27. M. S. Dresselhaus, G. Dresselhaus, R. Saito and A. Jorio, *Physics Reports-Review Section of Physics Letters*, 2005, 409, 47-99.
28. J. B. Li, Y. X. Huang, P. Chen and M. B. Chan-Park, *Chemistry of Materials*, 2013, 25, 4464-4470.
29. Q. Liu and J. Y. Zhang, *Langmuir*, 2013, 29, 3821-3828.
30. A. Morozan, P. Jegou, B. Jousselme and S. Palacin, *Physical Chemistry Chemical Physics*, 2011, 13, 21600-21607.
31. Z. H. Sheng, L. Shao, J. J. Chen, W. J. Bao, F. B. Wang and X. H. Xia, *Acs Nano*, 2011, 5, 4350-4358.

32. S. Li, D. Wu, H. Liang, J. Wang, X. Zhuang, Y. Mai, Y. Su and X. Feng, *ChemSusChem*, 2014, 7, 3002-3006.
33. G. Wu, Z. W. Chen, K. Artyushkova, F. H. Garzon and P. Zelenay, *Ecs Transactions*, 2008, 16, 159-170.
34. R. Huo, W. J. Jiang, S. Xu, F. Zhang and J. S. Hu, *Nanoscale*, 2014, 6, 203-206.
35. H. R. Byon, J. Suntivich and Y. Shao-Horn, *Chem Mater*, 2011, 23, 3421-3428.
36. Z. Y. Zhang, K. L. More, K. Sun, Z. L. Wu and W. Z. Li, *Chemistry of Materials*, 2011, 23, 1570-1577.
37. D. S. Yu, Q. Zhang and L. M. Dai, *J Am Chem Soc*, 2010, 132, 15127-15129.
38. L. T. Qu, Y. Liu, J. B. Baek and L. M. Dai, *Acs Nano*, 2010, 4, 1321-1326.